Journal of the Energy Institute 92 (2019) 82–93

Contents lists available at ScienceDirect

Journal of the Energy Institute

journal homepage: http://www.journals.elsevier.com/journal-of-the-energy-institute

Characterization of the physicochemical and structural evolution of biomass particles during combined pyrolysis and CO_2 gasification

John Eshun [a], Lijun Wang [b, c, *], Emmanuel Ansah [a], Abolghasem Shahbazi [b, c], Keith Schimmel [a], Vinayak Kabadi [c], Shyam Aravamudhan [d]

[a] Department of Energy and Environmental Systems, North Carolina Agricultural and Technical State University, 1601 East Market Street, Greensboro, NC 27411, USA
[b] Department of Natural Resources and Environmental Design, North Carolina Agricultural and Technical State University, 1601 East Market Street, Greensboro, NC 27411, USA
[c] Department of Chemical, Biological, and Bioengineering, North Carolina Agricultural and Technical State University, 1601 East Market Street, Greensboro, NC 27411, USA
[d] Joint School of Nanoscience and Nanoengineering, North Carolina Agricultural and Technical State University, 1601 East Market Street, Greensboro, NC 27411, USA

ARTICLE INFO

Article history:
Received 1 February 2017
Received in revised form
9 November 2017
Accepted 13 November 2017
Available online 21 November 2017

Keywords:
Biomass
Pyrolysis
CO_2 gasification
Biochar
Physicochemical properties

ABSTRACT

The combination of pyrolysis and CO_2 gasification was studied to synergistically improve the syngas yield and biochar quality. The subsequent 60-min CO_2 gasification at 800 °C after pyrolysis increased the syngas yield from 23.4% to 40.7% while decreasing the yields of biochar and bio-oil from 27.3% to 17.1% and from 49.3% to 42.2%, respectively. The BET area of the biochar obtained by the subsequent 60-min CO_2 gasification at 800 °C was 384.5 m^2/g, compared to 6.8 m^2/g for the biochar obtained by the 60-min pyrolysis at 800 °C, and 1.4 m^2/g for the raw biomass. The biochar obtained above 500 °C was virtually amorphous.

1. Introduction

Pyrolysis and gasification have been identified as economically-feasible and energy-efficient thermochemical technologies to convert biomass into bio-oil, syngas and biochar [1]. Pyrolysis can decompose biomass at an elevated temperature between 350 °C and 800 °C in the absence of air. The proportion and quality of the bio-oil, syngas and biochar from biomass pyrolysis depend on the characteristics of the biomass and the pyrolytic conditions. Gasification occurs at an elevated temperature between 550 °C and 1600 °C in the presence of a sub-stoichiometric amount of an oxidizing agent such as air, oxygen, steam or CO_2. During CO_2 biomass gasification, the CO_2 can be reduced to produce more CO through the Boudouard reaction ($CO_2 + C \rightarrow 2CO$), which provides a route for CO_2 sequestration [2]. The use of CO_2 as a gasifying agent has a potential to increase the efficiency of carbon conversion during biomass gasification [3]. CO_2 gasification of biomass also enables a more complete conversion of biomass to volatiles at a lower temperature [4]. The lower temperature for CO_2 gasification of biomass can occur at around 700 °C. The addition of CO_2 was found to improve biochar reactivity during gasification at a temperature below 900 °C [5]. Kwon et al. [6] investigated the effect of introducing CO_2 and N_2 in the pyrolysis process at 550 °C in a tubular reactor and found that the CO_2 led to a decrease of bio-oil yield and an increase of syngas.

During pyrolysis and gasification, biomass particles experience a complicated physicochemical and structural evolution to gradually form biochar when the volatiles in the biomass are released [7]. Biochar is an organic carbon that is highly porous in nature. It has a long

* Corresponding author. Department of Natural Resources and Environmental Design, North Carolina Agricultural and Technical State University, 1601 East Market Street, Greensboro, NC 27411, USA.
E-mail address: lwang@ncat.edu (L. Wang).

https://doi.org/10.1016/j.joei.2017.11.003
1743-9671/

residence time in soil due to its highly condensed aromatic structure resulting in high biochemical recalcitrance [8]. These properties contribute to biochar's efficiency in its industrial applications. Some of the industrial applications of biochar are to improve soil fertility by providing nutrients to the soil, increasing water retention, lowering soil acidity and density, and increasing microbial activity. The heating rate, temperature and biomass particle size play important roles in the physicochemical and structural evolution from biomass to biochar during pyrolysis [9]. On the other hand, the surface properties and structure of biochar have significant effects on the reactivity of the biochar during gasification and combustion [10,11]. Several studies were focused on investigating the effect of pyrolysis conditions such as heating rate and temperature on the physicochemical properties of biochar [12–16]. Temperature of pyrolysis has been found to have more significant effects on the physicochemical properties of biochar than the type of biomass materials [17].

Biomass pyrolysis generates two low-quality by-products of syngas and biochar; (1) The heating value of syngas produced from biomass pyrolysis is usually very low as CO_2 is the dominant compound in the syngas, and (2) the BET surface area of biochar from biomass pyrolysis is low which limits its application as an adsorbent [17,18]. Combined pyrolysis and CO_2 gasification was thus studied to synergistically improve the quality of syngas and biochar produced by biomass pyrolysis. Moreover, little research has been conducted to investigate the physicochemical and structural evolution of biomass particles with the increase in temperature during combined pyrolysis and CO_2 gasification. This research was thus to characterize the physicochemical and structural changes of biomass particles during the pyrolysis and subsequent gasification with CO_2 at a temperature from 100 °C to 800 °C.

2. Materials and experimental methods

2.1. Preparation of biomass feedstock

Sawdust mainly from poplar wood species, which was provided by Beard Hardwoods, Inc., (Greensboro, NC), was used as a representative biomass. The sawdust sample was dried and further ground in a Thomas Wiley mill with a 1 mm screen (Thomas Scientific, Swedesboro, NJ). The particle size distribution of the milled sample was measured according to the ASTM C136 standard. The fraction of the milled sample with particle sizes between 300 μm and 600 μm (average size of 450 μm), that accounted for 48% of the total mass, was used in the experiments.

2.2. Proximate and ultimate analyses of the biomass

Proximate analysis was carried out in a thermogravimeter (TGA) (TA Instruments SDT Q600). Approximately 10 mg of the sample was heated from the ambient temperature to 110 °C at a rate of 10 °C/min in the TGA with nitrogen at a flow rate of 60 ml/min as a carrier gas. The sample was isothermally held at 110 °C for 10 min to achieve a constant weight for the measurement of the moisture content. The sample was then heated to 700 °C at 20 °C/min and kept at 700 °C isothermally for 10 min to achieve a constant weight for the measurement of the content of volatiles. The carrier gas was then switched to air at 60 ml/min. The sample was heated to 900 °C at a rate of 20 °C/min to completely burn the leftover char for the measurement of the contents of fixed carbon and ash. The ultimate analysis was conducted on a CHNS/O Analyzer (Perkin Elmer 2400 series II) to determine the elemental composition of the biomass sample. The contents of C, H, S and N were determined directly while the O content was calculated as the difference. The higher heating values (HHV) of the raw biomass and biochar samples were measured using an oxygen bomb calorimeter (Model 1672, Parr Instrument, Moline, IL).

2.3. Combined pyrolysis and CO_2 gasification of biomass in a tubular reactor

Pyrolysis and gasification experiments were carried out in a stainless steel (#316) bench-scale tubular reactor of 30 cm in length and 1 cm in internal diameter as shown in Fig. 1. The reactor was charged with 10 g of the biomass sample. The sample was heated with an electric furnace to a final temperature ranging from 100 °C to 800 °C at a heating rate of 80 °C/min. The temperature was controlled within an

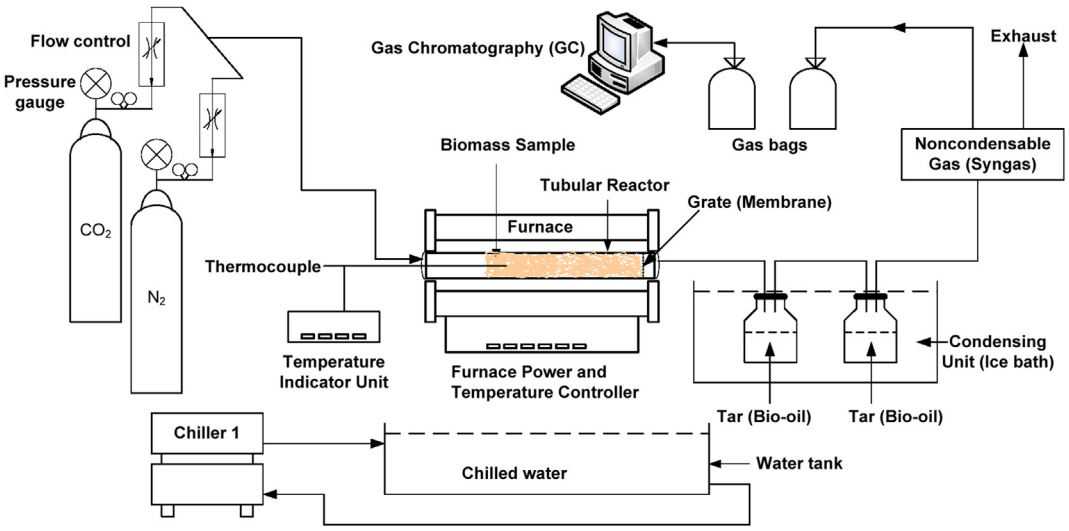

Fig. 1. Schematics of the tubular reactor unit for the preparation of biochar samples.

accuracy of ±2 °C by an in-built controller with a K-type thermocouple. Nitrogen at a flow rate of 0.23 L/min/g-biomass was used as a purging and carrier gas. The flow rate of the carrier gas was determined to be able to effectively separate the volatile gases from the biochar to avoid secondary reactions [19]. When the final temperature was reached, the carrier gas was switched to CO_2 at a flow rate of 0.23 L/min/g-biomass to further gasify the char with CO_2 at the final temperature for 60 min. Pyrolysis at each final temperature for 60 min was also conducted for comparison. The volatiles that existed from the reactor were passed through two 35 ml vials placed in series in an ice cooling bath (as shown in Fig. 1) to collect the condensable volatiles. At the end of the pyrolysis/gasification, the reactor was submerged into a cooling bath to be rapidly cooled down to the ambient temperature for less than 2 min. The solid biochar residue was recovered, weighed and stored in a refrigerator for further analyses. The masses of biochar and bio-oil were summed up and subtracted from the mass of the raw biomass to obtain the syngas or non-condensable gas (NCG) yield. The yields of biochar, bio-oil and NCG were then expressed as the percentages of the mass of the raw biomass.

2.4. Analyses of physical and chemical properties

2.4.1. FTIR analysis of chemical functional groups

The chemical functional groups of the raw and biochar samples were analyzed using a Shimadzu IR Prestige-21 Fourier transform infrared (FTIR) spectrophotometer with capabilities to perform attenuated total reflection (ATR) and sample/KBr mixture analyses. The solid raw biomass or biochar sample was first ground to fine powder to reduce scattering losses and absorption band distortions. The sample was then mixed with KBr at a sample to KBr mass ratio of 1:100. The mixture was manually ground and pressed into a translucent pelletized disc. The pelletized disc sample was placed in the path of the IR light, where spectra were collected over 200 scans of the sample in the range of 4000 cm^{-1}–400 cm^{-1} at a resolution of 4 cm^{-1}. The Happ-Genzel apodization function was used to achieve a good balance between ripple size and resolution.

2.4.2. Topographical analysis with SEM

The surface morphology and topography of the samples were analyzed by a scanning electron microscopy (SEM, Carl Zeiss Auriga-BU FIB SEM/EDS microscope) to determine the structural transformation from the biomass to biochar. To ensure good electrical conduction, the sample was first placed on an adhesive carbon tape mounted on an aluminum stub and coated with a sputter of Au–Pd using a Leica EM ACE200 vacuum electric sputter coater. The coated sample was then placed in the scanning electron microscope for imaging at a 3 kV beam voltage.

2.4.3. Physisorption analysis with BET

The pore size distribution, total pore volume and surface area of the biomass and biochar samples were measured with a surface area and pore analyzer (Micromeritics ASAP 2020). Prior to the gas adsorption measurements, the biomass and biochar samples were first dried in an air oven at 105 °C for 12 h. The dry samples were degassed at a temperature of 110 °C for 4 h. The degassed sample was then subjected to physisorption analysis using N_2 as the adsorptive gas at 77 K and relative pressure range of 0.01–1. The multilayer adsorption model developed by Brunauer-Emmett-Teller (BET) was used to evaluate the surface area (S_{BET}) while the pore size distribution of the sample was evaluated using the Barrett-Joyner-Halenda (BJH) model. The total pore volume was calculated from the amount of gas adsorbed at the required relative pressure. To ensure reproducibility and accuracy of the analysis, the experiments were repeated three times.

2.4.4. Crystallographic analysis with XRD

The degree of crystallinity of mineral materials in the samples was characterized by an X-ray Diffraction (XRD) analyzer (D8 DISCOVER X-ray diffractometer, Bruker Optics, Inc., Billerica, MA). The diffraction spectra were recorded in a 2θ angle range of 18°–50° with a PSD detector at a scanning rate of 0.014°/s. Cu Kα radiation (λ = 1.54 Å) generated at 40 mA and 40 kV was used as the X-ray source.

2.4.5. Molecular structural analysis with Raman spectroscopy

Raman spectra were measured at a constant room temperature using a Raman microscope with back scattering configuration (Horiba Jobin Yvon Technology) to characterize the molecular structural features of the samples. The source of the radiation was a laser operated at a 532 nm excitation wavelength. The laser was focused through a microscope with a 50× objective at a spectral resolution of 4 cm^{-1}, employing 10% laser power and 5 s of exposure time with a total of 15 acquisitions. The spectra were collected in the range from 200 cm^{-1}–3600 cm^{-1} and analyzed from 750 cm^{-1}–2250 cm^{-1}. Each sample was measured at three different sampling points, though the grinding was thorough and uniform enough to ensure an almost identical testing result from each point.

3. Results and discussion

3.1. Yields of biochar, bio-oil and non-condensable gases obtained in a tubular fixed bed reactor at different pyrolysis-gasification temperatures

As shown in Table 1, the raw sawdust contained 8.37% moisture, 77.93% volatiles, 12.08% fixed carbon and 1.62% ash. Fig. 2 shows the product distribution of the biochar, bio-oil and non-condensable gases as a function of the temperature for both biomass pyrolysis and

Table 1
Proximate, ultimate and energy content of raw sawdust biomass.

Sample	Proximate analysis wt% (air-dried at 35 °C)				Ultimate analysis wt% (air-dried at 35 °C)					HHV, MJ/kg (dry basis)
	Moisture	Volatile matter	Fixed carbon	Ash	C	H	N	S	O[a]	
Sawdust biomass	8.37	77.93	12.08	1.62	40.84	6.37	0.50	0.79	51.50	15.78

[a] Obtained by difference.

combined biomass pyrolysis and CO_2 gasification, both of which were held at the final temperature for 60 min. As shown in Fig. 2, no organic bio-oil compounds and syngas were generated at 100 °C and 200 °C and the weight losses that were about 9.9%–11.5% of the original masses at these temperatures were mainly caused by drying. Small volatile molecules started to be generated when the pyrolysis temperature further increased to 300 °C. The tar collected at 300 °C was 10.8% of the original mass of the biomass, which was contributed by the water in the biomass. The yield of non-condensable gas was 6.9% at pyrolysis temperature of 300 °C. When the temperature was further increased, the yields of non-condensable gases and bio-oil increased while the yield of biochar decreased. When the temperature increased from 300 °C to 800 °C during the pyrolysis-only, the yields of syngas and bio-oil increased from 6.9% to 23.4%, and from 10.8% to 49.3%, respectively, while the yield of biochar decreased from 82.3% to 27.3% as shown in Fig. 2a. The increase of syngas yield with the pyrolysis temperature was attributed to thermal decomposition of the biomass and part of tar. At a temperature above 500 °C, the secondary reactions of volatiles such as thermal cracking, methanation and water-gas shift reactions were also responsible for the increase in syngas yield. When the biochar was gasified with CO_2 at 300 °C for 60 min, the yields of syngas, bio-oil and biochar, as shown in Fig. 2b, were 10.5%, 7.9% and 81.6%, respectively, compared to 6.9%, 10.8% and 82.3% for pyrolysis-only at 300 °C for 60 min. Thus, the subsequent CO_2 environment at 300 °C did not significantly decrease the biochar yield. The increase of syngas yield and the decrease of liquid yield for the combined pyrolysis and CO_2 gasification at 300 °C might be caused by the decrease of the condensation of water vapor in CO_2. However, the subsequent CO_2 gasification at a higher temperature could significantly increase the syngas yield and decrease the biochar yield. The syngas yield for the combined pyrolysis and CO_2 gasification at 800 °C for 60 min was as high as 40.7%, compared to 23.4% for the pyrolysis-only at 800 °C for 60 min. The yield of biochar for the combined pyrolysis and CO_2 gasification at 800 °C was 17.1%, compared to 27.3% for the pyrolysis-only. The final weight of 17.1% at 800 °C after 60 min isothermal gasification showed that CO_2 gasification efficiency in the tubular reactor was improved with increasing temperature. During biomass gasification, CO is mainly released by breaking of carbonyl and carboxyl groups. However, during char CO_2 gasification, the CO_2 was reduced to CO while the char was oxidized to CO as shown in Eq. (1):

$$CO_2 + C \rightarrow 2CO \quad (1)$$

It was reported that the nascent char obtained in fast coal pyrolysis was very reactive to CO_2 and that the char gasification with CO_2, as shown in Eq. (1), occurred simultaneously with the tar thermal cracking, as indicated in Eq. (2) [20]. Moreover, the CO_2 can prevent tar polymerization to form char [21].

$$C_nH_m + nCO_2 \rightarrow 2nCO + (m/2)H_2 \quad (2)$$

CO_2 can also react with hydrogen molecules through the reverse water gas shift reaction (rWGS), as shown in Eq. (3), which is the dominant gas-gas reaction at a temperature higher than 700 °C [21]:

$$CO_2 + H_2 \rightarrow H_2O + CO \ \Delta H = 41.2 \text{ KJ/mol} \quad (3)$$

The bio-oil yield from the combined pyrolysis and CO_2 gasification was lower than that of pyrolysis-only at the same temperature for 60 min. Heavy-molecular-weight compounds of pyrolysis vapor are known to become active at a high temperature (e.g. 500 °C) through secondary reactions [22]. The bio-oil yield increased from 10.8% at 300 °C to 49.3% at 800 °C for the pyrolysis-only while an increase from 7.9% at 300 °C to 42.2% at 800 °C for the combined pyrolysis and CO_2 gasification was observed. The combined pyrolysis-CO_2 gasification led to the production of more syngas and less char compared to the pyrolysis-only study, which is mainly due to the CO_2 reactivity with the biochar. The lower bio-oil production in the combined pyrolysis-CO_2 gasification compared to the pyrolysis-only at the same temperature for 60 min is attributed to tar cracking with the CO_2. The slight increase of the bio-oil yield for the combined pyrolysis-CO_2 gasification when the temperature increased from 700 °C to 800 °C might be caused by the increase in the oxidation of some product gases with CO_2 to form H_2O at a very high temperature (i.e. 800 °C).

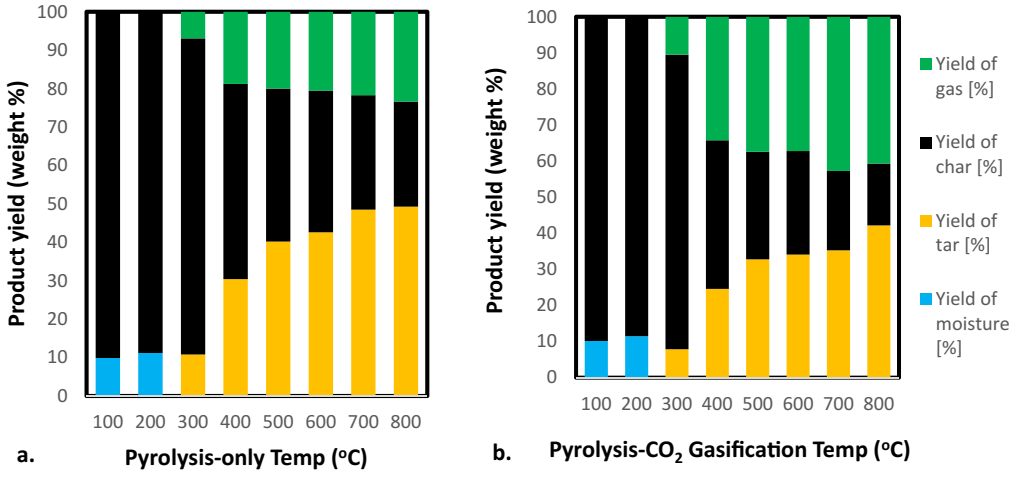

Fig. 2. Yields of biochar, bio-oil and non-condensable gases at different final temperatures for a) pyrolysis-only, and b) pyrolysis-60 min CO_2 gasification.

3.2. Change of elemental compositions from biomass to biochar

Table 2 gives the elemental compositions of the biochar collected at different temperatures during the pyrolysis-only and the combined pyrolysis-gasification in the tubular reactor. The biochar collected at higher temperature became more carbonaceous for both cases but the carbon content of the biochar produced by the combined pyrolysis-gasification was higher than that of the biochar produced by the pyrolysis-only at the same temperature above 400 °C. During the pyrolysis and the pyrolysis-CO_2 gasification processes, the increase in temperature caused more and more hydrogen and oxygen in the biomass to be released and form hydrogenated and oxygenated compounds in the syngas and bio-oil. The carbon content of the biochar increased from 44.98 wt% at 100 °C to 75.09 wt% at 800 °C while hydrogen content decreased from 6.96 wt% at 100 °C to 2.58 wt% at 800 °C for the pyprolysis-only. For the pyrolysis-CO_2 gasification, the carbon content of the biochar increased from 44.72 wt% at 100 °C to 82.45 wt% at 800 °C while hydrogen content decreased from 6.70 wt% at 100 °C to 1.20 wt% at 800 °C. The CO_2 gasification of the char destroys the hydrogen-containing char structure and promotes cracking of the benzene ring and fracturing of hydroxyl, methyl and methylene groups. It also weakens the interaction between hydrogen and char matrix causing an increase in hydrogen fluidity and radicals [23]. However, most of the hydrogen radicals combine with other free radical fragments generated from the fracture of the biochar macromolecules to produce more volatiles. The oxygen in biochar decreased from 48.74 wt% at 100 °C to 19.91 wt% at 800 °C for the pyprolysis-only while for the pyrolysis-gasification, it decreased from 47.45 wt% at 100 °C to 15.43 wt% at 800 °C. Nitrogen and sulfur in the biomass were less than 1%. Nitrogen content generally decreased with increasing temperature for both cases because as temperature increased more nitrogen in the biomass was released to form volatile compounds such as HCN, NH_3 and NO_x. The slight increases at 500 °C and 600 °C (from 0.06 to 0.51%) and at 700 °C and 800 °C (from 0.12 to 0.68%) for the pyrolysis-CO_2 gasification are most likely ascribed to the chemical heterogeneity of the initial biomass since some of the nitrogen in the char are released by heterogeneous oxidation.

Fig. 3 shows the Van Krevelen plot for the changes of the elemental ratios of H/C and O/C in the biochar collected at different temperatures and the raw biomass. This plot explains the degree of aromaticity and bonding arrangements during thermochemical conversion of biomass. These ratios indicate the degree of carbonization and thermochemical alterations that lead to fused aromatic ring structures in the material. There were significant decreases in the H/C and O/C atomic ratios with increase of the process temperature during the pyrolysis and gasification. The raw biomass had a relatively high H/C atomic ratio of 1.87, which implies that the raw biomass had low aromatic and high aliphatic content. The decrease of H/C ratio with the increase of temperature led to the formation of more aromatic structures. The highest decrease in H/C and O/C ratios occurred when the temperature increased from 300 °C to 400 °C as shown in Fig. 4. The relatively high ratios of H/C and O/C in the raw biomass and the biochar samples collected at a temperature below 300 °C were attributed to the presence of carbohydrates and some residual organic matters. The H/C and O/C of the biochar collected at a high temperature from 600 °C to 800 °C were close to those of coal and anthracite. The decrease in the H/C and O/C ratios with increasing temperature increased the degree of carbonization of the biochar, forming more graphitic structure in the biochar [24,25]. Biomass has a high oxygen content but the oxygen consumes part of the hydrogen in the biomass to produce water during thermochemical conversion. Therefore, the high H/C ratio in biomass did not result in high syngas yield during the pyrolysis and gasification due to the presence of a large amount of oxygen in the biomass [26]. However, the simultaneous decrease in H/C and O/C ratios with the increase of the temperature from 100 °C to 800 °C increased the high heating value (HHV) of the biochar, as shown in Fig. 4. The HHV increased from 18.39 MJ/kg for the biochar collected at 100 °C to 30.64 MJ/kg at 800 °C. As the yield of the biochar from the combined pyrolysis and gasification at 800 °C was 17.1% of the original dry mass, the biochar contained 28.5% of the initial energy in the raw biomass.

3.3. Change in chemical functional groups during combined pyrolysis and CO_2 gasification

Fig. 5 presents the FTIR spectra of the raw biomass and the biochar obtained at different temperatures during the combined pyrolysis and CO_2 gasification. The absorption band spectra in the diagnostic region (4500 cm^{-1} to ~1500 cm^{-1}) are characteristic of the functional groups or bond types in the raw biomass and biochar samples and the fingerprint region (~1500 cm^{-1} to 400 cm^{-1}) shows the intramolecular reactions within the biomass and biochar. The spectra were characterized by several principal bands which suggest the presence of a variety of oxygen functional groups and aromatic carbon groups in oxygenated hydrocarbons found in cellulosic biomass. This observation denotes that most of the surface functional groups were destroyed along the heat treatment and an almost carbonaceous solid product was obtained. As shown in Fig. 5, a broad band existing between 3600 $cm^{-1}$and 3250 cm^{-1} with a peak at 3360 cm^{-1} was attributed to the presence of O–H functional group in raw lignocellulosic biomass and biochar collected at a temperature below 300 °C. However, the O–H band intensity gradually decreased with increase in temperature higher than 300 °C and almost disappeared in the biochar collected at the temperature

Table 2
Elemental composition of biochar collected at different temperatures during pyrolysis-only and pyrolysis-subsequent 60 min CO_2 gasification (%, dry mass basis).

		Final temperature for pyrolysis-only and pyrolysis-subsequent 60 min CO_2 gasification (°C)							
		100	200	300	400	500	600	700	800
Carbon (%)	*Py-only*	44.98	48.67	50.93	60.28	66.11	71.73	73.41	75.09
	Py-CO_2	44.72	48.33	49.01	62.80	70.47	74.24	79.53	82.45
Hydrogen (%)	*Py-only*	6.96	6.48	6.37	4.91	4.22	2.92	2.81	2.58
	Py-CO_2	6.70	5.98	5.73	4.68	3.41	2.19	2.23	1.20
Nitrogen (%)	*Py-only*	0.56	0.53	0.51	0.49	0.47	0.32	0.26	0.19
	Py-CO_2	0.25	0.24	0.20	0.07	0.06	0.51	0.12	0.68
Sulfur (%)	*Py-only*	0.75	0.89	0.67	0.53	0.62	0.57	0.42	0.46
	Py-CO_2	0.88	0.87	0.76	0.44	0.59	0.45	0.31	0.23
Oxygen (%)	*Py-only*	48.74	44.43	43.95	33.82	30.14	29.33	23.78	19.91
	Py-CO_2	47.45	44.59	43.30	32.01	25.47	22.61	17.81	15.43

Py-only = Pyrolysis-only, Py-CO_2 = Pyrolysis-CO_2 gasification.

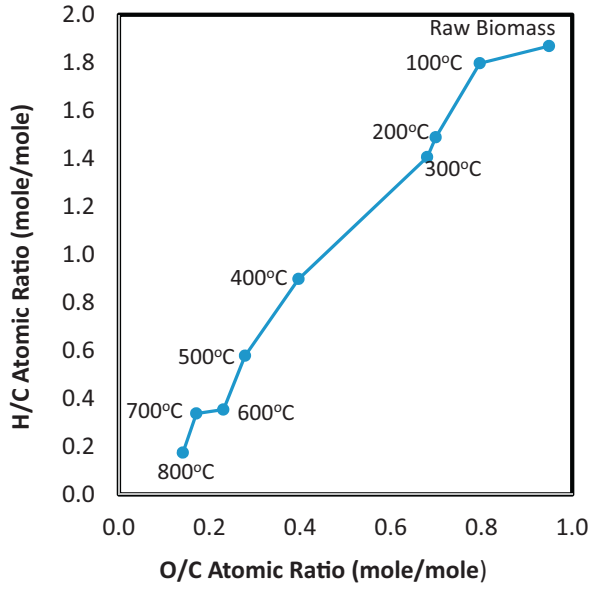

Fig. 3. Van Krevelen plot for raw biomass and biochar collected at different temperatures during pyrolysis and subsequent 60 min CO_2 gasification.

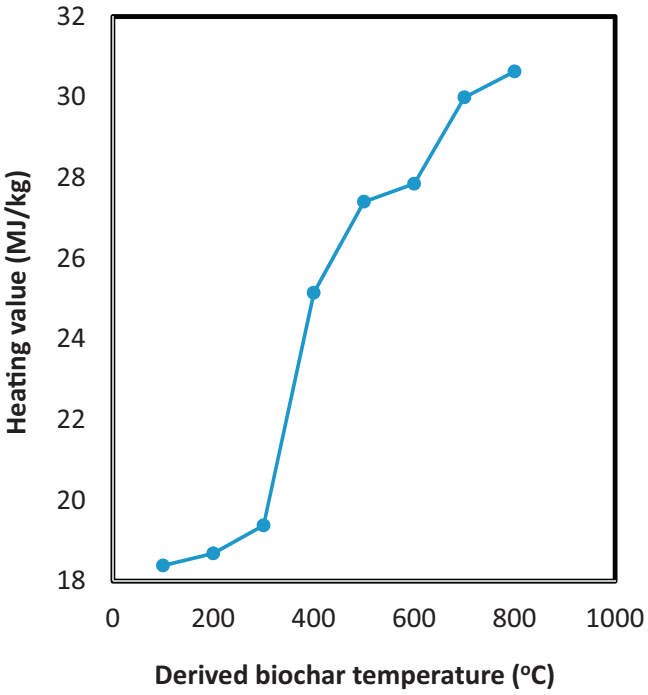

Fig. 4. Higher heating values of biomass and biochar collected at different temperatures during pyrolysis and subsequent 60 min CO_2 gasification.

above 600 °C due to the acceleration of dehydration reaction. The absorbance band at 3000 cm^{-1} – 2750 cm^{-1} with a peak at 2900 cm^{-1} contributed by the aliphatic C–H stretching vibration and the band at 2250–1955 cm^{-1} with a peak at 2100 cm^{-1} was caused by the stretching vibrations of carboxyl and carbonyl C=O functional groups. There were also a number of bands between 1750 cm^{-1} and 1500 cm^{-1}, which were attributed to aliphatic and olefinic C–H bending as well as aromatic C=C stretching vibrations. It might also contain –OH in-plane bending modes, carbonyl (C=O) and other common alkane and oxygenated hydrocarbon functional groups in the biomass and biochar. Bai et al. [27] indicated that the CO_2 atmosphere of thermochemical conversion of biomass increased the content of aliphatic C–H groups and the concentration of methylene C–H bands compared to the N_2 atmosphere. During the pyrolysis and gasification, the biomass was transformed from aliphatic structure to aromatic structure with increasing temperature. The FTIR spectra show increasing degree of condensation and aromaticity of the biochars with increasing temperature as the intensities of the bands between 1750 cm^{-1} and 1500 cm^{-1} decreased with increase in temperature. The intense band occurring around 1040 cm^{-1} was caused by the C–C–O or C–*O*–C

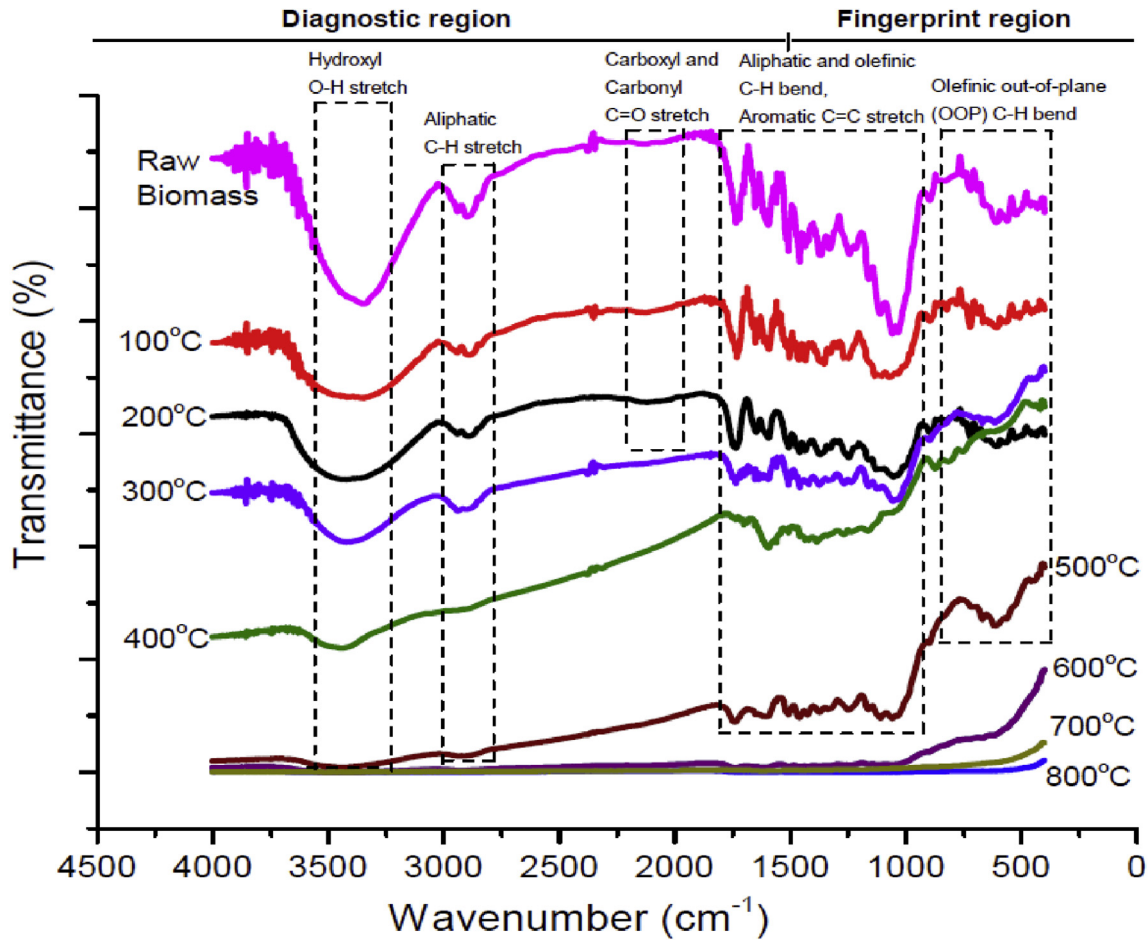

Fig. 5. FTIR Spectra of the raw biomass and biochar collected at different temperatures during pyrolysis and subsequent 60 min CO_2 gasification.

asymmetric stretching vibration [28]. The smaller bands around 750 cm^{-1}–450 cm^{-1} with a peak at 620 cm^{-1}, might be due to olefinic out-of-plane (oop) C–H bending modes.

3.4. Topographical evolution from biomass to biochar

Fig. 6 shows the SEM images of the morphological changes from the raw biomass to the biochar collected at different temperatures for the pyrolysis-only and the combined pyrolysis and CO_2 gasification. The raw biomass particles were mostly regular in sizes and contained few and unnoticeable pores on the surface structure. The biochar particles, on the other hand, were observed to be generally irregular and became more porous as the process temperature increased from 100 °C to 800 °C. Furthermore, as the temperature increased, aligned honeycomb-like groups of pores and large channel-like structures proliferated on the surface of the biochar, showing at least partial retention of the capillary structure of the raw biomass. They originated most likely from biological capillary structure of the raw sawdust. The mechanical intensity exerted by the pyrolysis-CO_2 gasification temperature influenced the biochar structure and the effect became more pronounced as the temperature increased from 500 °C to 800 °C compared to that of the pyrolysis-only study, as illustrated by the SEM images. The changes in both instances were attributed to dehydration and devolatilization. As the volatiles escaped, pores and cracks began to develop on the surface of the biochar, resulting in rough and irregular surface. However, the devolatilization in CO_2 gasification resulted in more pores in the biochar compared to the pyrolysis-only due to the reaction of CO_2 with the biochar to produce more volatiles. The biochars obtained at a final temperature from 600 °C to 800 °C had the most irregular and distorted surfaces with many pores. The porosity of the biochar increased with the pyrolysis-gasification temperature, which could enhance the reactivity of the biochar. Other researchers also reported that biomass derived chars were more reactive than coal-derived chars, which was caused by the superior porosity and high surface area of biochar as well as the availability of inherent catalytic elements such as sodium (Na), calcium (Ca) and potassium (K) [29].

3.5. BET surface area, pore volume and pore size distribution

Table 3 provides the BET surface areas, total pore volume and pore size, which were measured for the raw biomass and biochar generated from 100 °C to 800 °C during pyrolysis-only and combined pyrolysis and CO_2 gasification. The data presented in Table 3 for both the pyrolysis-only and the combined pyrolysis and CO_2 gasification are the average values from three experiments with relative standard deviation (RSD) values within the ranges of 4.5–12.7% for the BET surface areas, 3.8–10.3% for the total pore volumes and 5.6–14.8% for the pore sizes. The pyrolysis itself could not produce biochar with high BET surface area and pore volume. As shown in Table 3, the BET surface

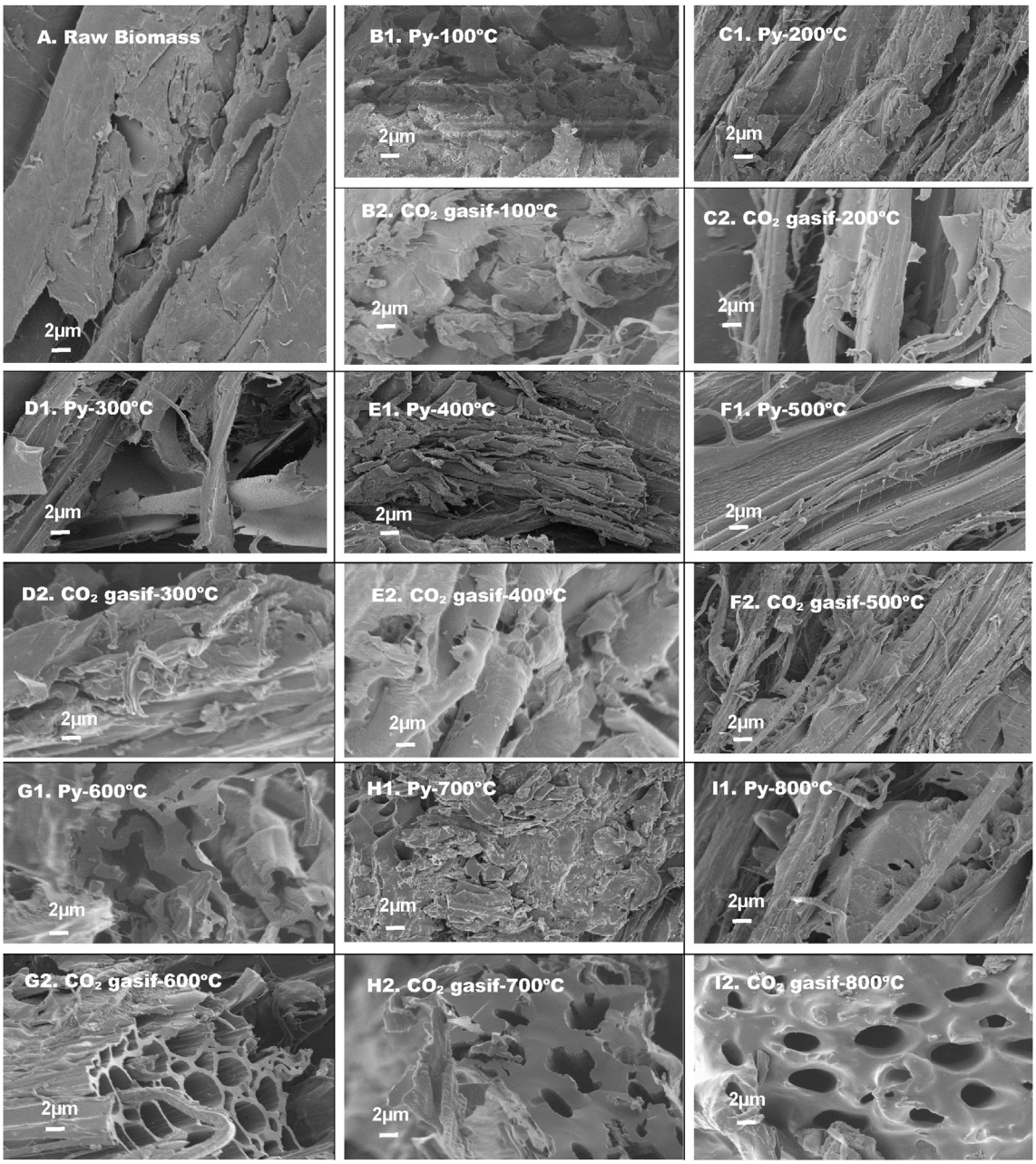

Fig. 6. Comparison of SEM images of raw biomass and biochar collected at different temperatures between pyrolysis-only and pyrolysis-subsequent 60 min CO_2 gasification.

Table 3
BET Surface area, total pore volume and adsorption average pore size for raw biomass and biochar collected at different temperatures during pyrolysis-only and pyrolysis-subsequent 60 min CO_2 gasification.

		BET surface area (m^2/g)		Total pore volume ($cm^3/g \times 10^{-3}$)		Average pore size (nm)	
		Pyrolysis-only	Pyrolysis-CO_2 gasification	Pyrolysis-only	Pyrolysis-CO_2 gasification	Pyrolysis-only	Pyrolysis-CO_2 gasification
Raw Biomass		1.4	1.2	3.135	3.005	8.87	10.49
Biochar collected at different temperatures (°C)	100	1.3	2.0	2.746	3.703	8.22	7.41
	200	2.3	2.4	2.943	3.875	5.23	6.47
	300	2.3	3.9	4.030	4.794	6.80	4.95
	400	2.8	37.4	4.359	23.72	6.35	2.53
	500	3.2	99.2	4.414	57.18	5.60	2.32
	600	3.9	140.8	5.796	96.79	5.92	2.75
	700	4.5	255.5	6.691	150.7	5.37	2.36
	800	6.8	384.5	5.640	223.7	3.34	2.33

area of the biochar collected from the pyrolysis-only at 800 °C for 60 min was only 6.8 m^2/g, compared to 1.4 m^2/g for the raw biomass and 2.3 m^2/g for the biochar collected at 300 °C. The surface area and total pore volumes increased with increase in the pyrolysis-gasification temperature. The BET surface area and total pore volume did not increase significantly when the pyrolysis-gasification temperature increased from 100 °C to 300 °C. The BET surface area of the raw biomass, biochar at 100 °C, 200 °C, and 300 °C were 1.2 m^2/g, 2.0 m^2/g, 2.4 m^2/g and 3.9 m^2/g respectively. However, when the temperature was raised to 400 °C, the BET surface area increased drastically to 37.4 m^2/g while the total pore volume increased to 23.72× 10^{-3} cm^3/g. The drastic increase in the BET surface area during the pyrolysis-gasification, when the temperature increased from 300 °C to 400 °C, might be caused by the opening up of the carbon crystals at high temperature and the violent devolatilization in CO_2 gasification. That is, the subsequent CO_2 gasification generated more pores. When the temperature was further increased to 800 °C, the BET surface area was 384.5m^2/g and the pore volume became 223.7 × 10^{-3} cm^3/g. During pyrolysis and gasification, the average pore size decreased with increase in temperature. Biochar obtained from CO_2 gasification at a high temperature was highly porous. At lower temperatures, however, there were less pores with bigger sizes, as shown in Table 3. The average pore size distribution was between 2.3 nm and 10.5 nm. The small pores and high surface area of the biochar obtained by the subsequent CO_2 gasification at a high temperature could increase the potential efficiency of the biochar for the recovery of fertilizer nutrients in wastewater and the water holding capacity of the biochar as a soil conditioner.

3.6. Crystallographic evolution during pyrolysis and gasification

Fig. 7 displays the XRD profiles for the raw biomass and the biochar collected at different temperatures. The XRD diffractrogram shows the crystallinity of the material by depicting the intensity of the diffracted beam as a function of the Bragg angle, 2θ examined over the range of 18°–50°. Two narrow pronounced and intense peaks were detected at the 2θ angles at around 20.86° and 26.60° for the biochars generated from 200 °C to 400 °C. These peaks might be ascribed to the crystallinity in lattice spacing of cellulose, which are orderly arranged as a result of the thermochemical process. They correspond to diffuse graphite (002) and (100) peaks in low and high 2θ regions, respectively [30]. The (002) peak, which is theoretically symmetric, as depicted in Fig. 7, is imputable to parallel packing of carbon layers with distances between layers in a stack arrangement. The (100) peak is interpreted as the result of two-dimensional reflection of X-ray from carbon layers, which also turns to characterize the aromaticity of the char [31]. Tsai et al. [32] attributed the peak around 26.60° to the presence of quartz (SiO_2). This study highlights an important observation that the crystallinity in lattice spacing of the woody sawdust biomass occurred at temperatures ranging from 200 °C to 400 °C, reflecting the thermal stability of cellulose at this temperature range. Kloss et al. [33] found the presence of calcium oxalate mineral, whewellite ($CaC_2O_4.H_2O$) structure in the feedstock of poplar wood and its biochar produced at 400 °C, which disappeared at 525 °C and were completely replaced by calcite. Fig. 7 shows that the intensity of the peaks at 20.86° and 26.60° reduced dramatically for the biochar collected at 500 °C. This is due to the reduction in crystallinity of the biochar as a result of low intensity of cellulose structures in the biochar at these high temperatures. As the temperature increased above 500 °C, the peak at 20.86° totally

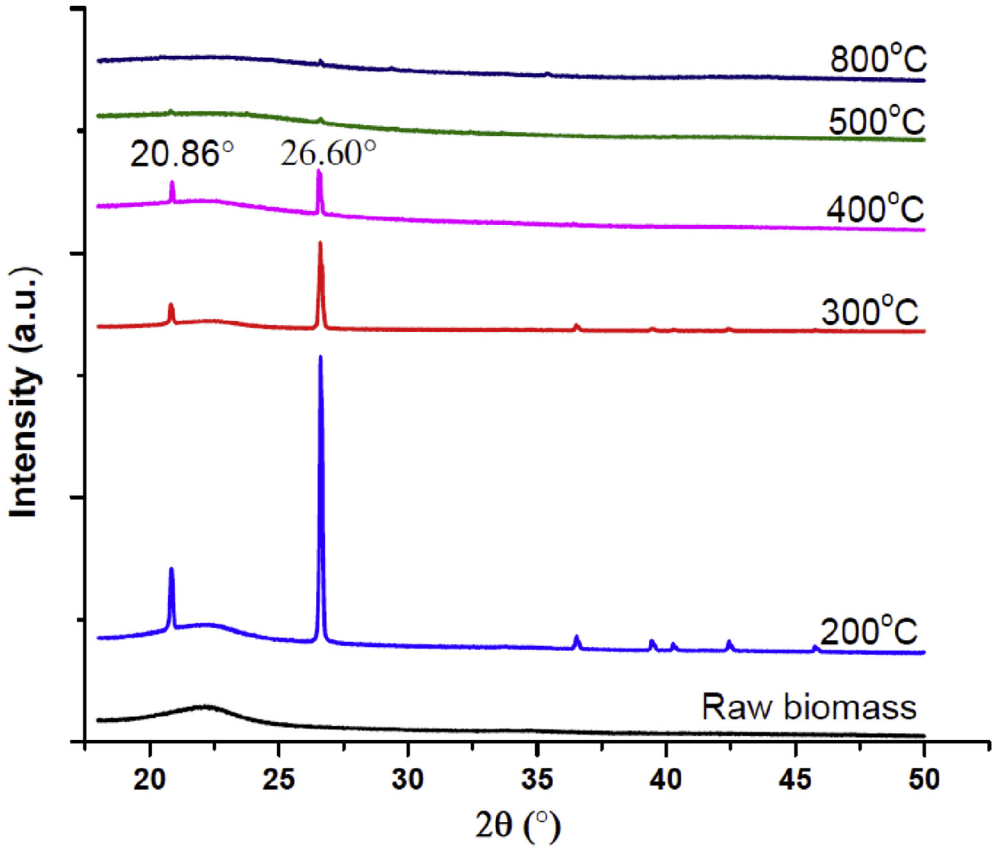

Fig. 7. XRD patterns of biomass and biochar at different temperatures for pyrolysis-60 min CO_2 gasification.

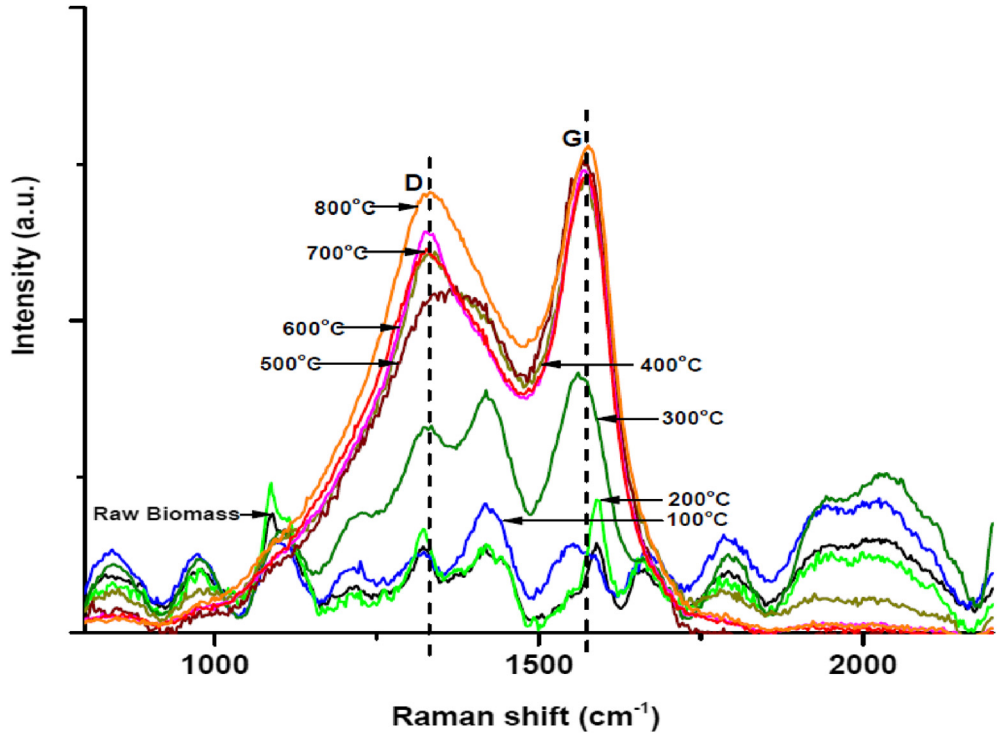

Fig. 8. Raman spectra for raw biomass and biochar at different temperatures for pyrolysis-60 min CO_2 gasification.

disappeared, which is attributed mainly to the complete decomposition of cellulose at a high temperature. Unlike cellulose, hemicellulose and lignin in the biochar are both known to be non-crystalline or amorphous in nature. Biochar obtained at 500 °C and above in this study is, therefore, virtually amorphous. The amorphous carbon in the biochar represents non-aromatic carbon trapped in the biomass macromolecules. Upon high heat treatment, the association between the amorphous carbon and the macromolecules breaks, releasing the amorphous carbon. The two intense peaks were non-existent in the raw biomass. However, there was a broader peak at 22.60° for the raw biomass. This peak is attributed to the fact that the cellulose structure in the raw biomass, which has not undergone any thermal changes, has a disordered lattice spacing and, therefore, non-crystalline in nature.

3.7. Change in molecular structure during pyrolysis and gasification

Raman spectra characteristics in the range of 750 cm^{-1} to 2250 cm^{-1} were selected in this study. Fig. 8 provides the spectra of the raw biomass and the biochars from 100 °C to 800 °C. The D band found at ~1350 cm^{-1} is attributed to defect structures in the highly ordered carbonaceous biochar. The D-band may be assigned to the condensed benzene rings in the amorphous (partially hydrogenated) carbon films [34]. It may also be due to graphitic lattice vibration mode with A_{1g} symmetry [35]. The D-band can further be linked to the breathing modes of disordered graphite ring in the biochar [36]. The G band was found at ~1580 cm^{-1} and is an evidence of the vibrations of crystallite sp^2 carbon atoms found in the graphitic materials and double bonds in the biochar. The G band may be attributed to the aromatic ring systems in the biochar [34]. It may also be due to an ideal graphite lattice vibration mode with E_{2g} symmetry [35]. With increase in the pyrolysis-gasification temperature, the intensities of both the D and G bands increased mainly due to the increase in the light absorbing capacity of the biochar, reflecting the loss of O-containing functional groups and changes in the relative concentrations of small and large aromatic ring systems [34]. The intensities of the D bands, however, increased progressively more than the G bands as the temperature increased, indicating gradual increase in the degree of disorderliness. The I_D/I_G ratio based on integral intensity (area under the peak) was calculated by modelling the peaks according to a model presented by Sadezky et al. [35] for curve fitting with band combinations of first-order Raman spectra generated at 514 nm wavelength. The relationship between the I_D/I_G ratio and the changes in temperature is depicted in Fig. 9. The I_D/I_G ratio increased initially from 2.21 for the raw biomass to 3.84 at 100 °C and then decreased monotonously to 1.05 at 300 °C before increasing progressively to 2.65 at 800 °C. The 1.05 at 300 °C threshold may be attributed to a change in structural evolution from ordering of sp^2 crystallite carbon structures to depolymerisation. The increasing trend in I_D/I_G ratio with increasing temperature beyond 300 °C could most likely reflect at least two different structural evolutions presented in this study: 1) The reduction in crystallinity of the biochar and increase in the amorphization phase. High carbonization temperature causes the graphite-like crystallites to become disordered and amorphous. 2) The relative increases in the concentrations of aromatic rings having six or more fused benzene rings as a result of dehydrogenation of hydroaromatics and the growth of aromatic rings in the char [34]. The first hypothesis is the least likely, as increasing temperature is known to increase the order of the carbonaceous materials.

4. Conclusions

The subsequent CO_2 gasification immediately after pyrolysis at a temperature higher than 300 °C could significantly increase the yield of syngas and improve the quality of biochar with high BET surface area and pore volume but decrease the yields of bio-oil and biochar. The

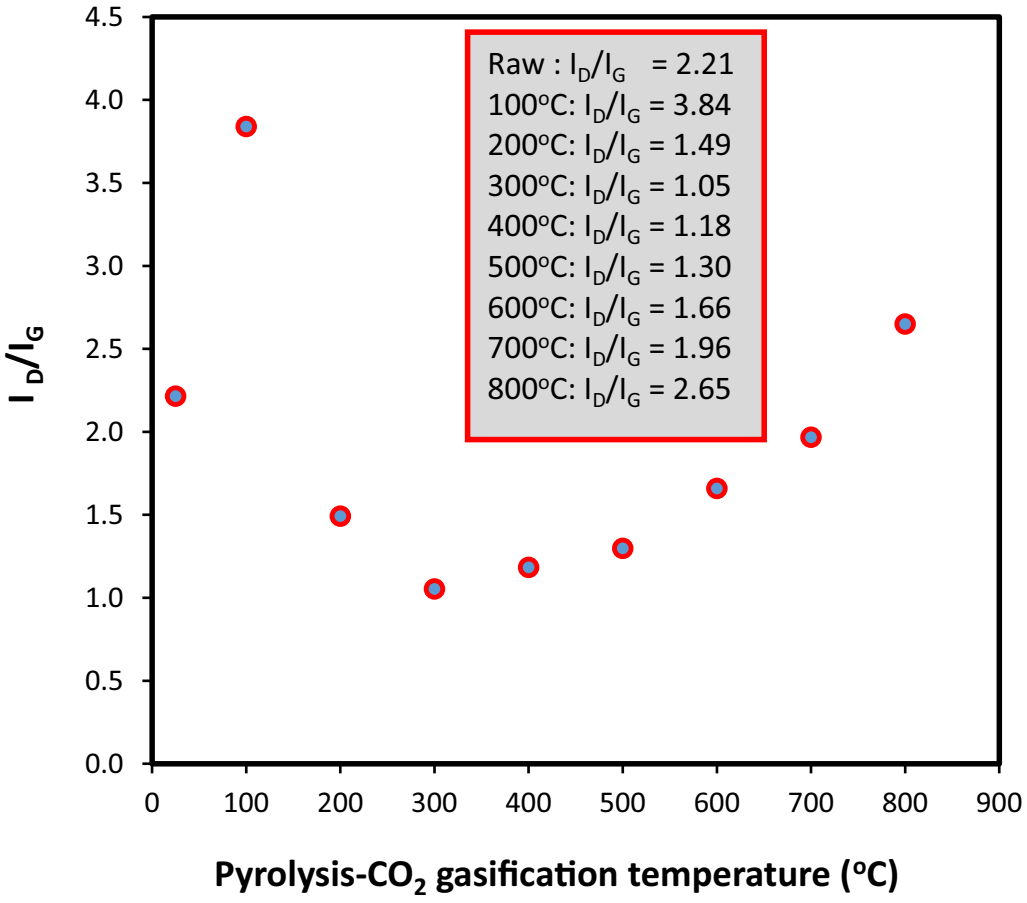

Fig. 9. I_D/I_G versus temperature for pyrolysis-60 min CO_2 gasification.

syngas yield for the combined pyrolysis and CO_2 gasification at 800 °C for 60 min was 40.7%, compared to 23.4% for the pyrolysis-only at 800 °C for 60 min. The yields of biochar and bio-oil for the combined pyrolysis and CO_2 gasification at 800 °C were 17.1% and 42.2%, respectively, compared to 27.3% and 49.3% for the pyrolysis-only at 800 °C. The BET surface area and pore volume of the biochar obtained from the combined pyrolysis and gasification at 800 °C were 384.5 m^2/g and 223.7 $\times$ 10^{-3} cm^3/g, compared to 6.8 m^2/g and 5.640 $\times$ 10^{-3} cm^3/g for the biochar obtained by the pyrolysis-only at 800 °C, and 1.4 m^2/g and 3.135 $\times$ 10^{-3} cm^3/g for the raw biomass. The increase of process temperature decreased the H/C and O/C ratios and increased the heating value of the biochar. The FTIR spectra showed that the hydroxyl, aliphatic C—H, carbonyl and olefinic C═C groups in raw biomass gradually disappeared when the temperature was increased from 300 °C and above. Meanwhile, the SEM images showed gradual development of well-defined pores distributed on the surface of the biochar when the temperature increased from 100 °C to 800 °C. The XRD profiles confirmed the presence of two narrow pronounced and intense peaks at the 2θ angles of 20.86° and 26.60° for the biochars generated from 200 °C to 400 °C. As the pyrolysis-gasification temperature increased above 500 °C, the biochar displayed distinctive amorphous characteristics. The Raman spectra further verified that there was an increase in amorphization phase and existence of highly disordered graphitic-like crystallites for the biochar collected at a temperature higher than 300 °C.

Acknowledgements

A contribution of North Carolina Agricultural and Technical State University, supported by funds fully provided by U.S National Scientific Foundation (Grant #: HRD-1242152). Mention of a trade name, proprietary products, or company name is for presentation clarity and does not imply endorsement by the authors or the university. The authors would like to thank Dr. Vishwanath Deshmane, Dr. Svitlana Fialkova, Dr. Alex Aboagye, Dr. Richard Abrokwah and Dr. Talal Ahmed for their assistance in the sample analyses.

References

[1] T. Chen, J. Wu, Z. Zhang, M. Zhu, L. Sun, J. Wu, D. Zhang, Key thermal events during pyrolysis and CO_2-gasification of selected combustible solid wastes in a thermogravimetric analyser, Fuel 137 (2014) 77–84.
[2] G. Skodras, G. Nenes, N. Zafeiriou, Low rank coal – CO_2 gasification: experimental study, analysis of the kinetic parameters by Weibull distribution and compensation effect, Appl. Therm. Eng. 74 (2015) 111–118.
[3] E. Veca, A. Adrover, Isothermal kinetics of char-coal gasification with pure CO_2, Fuel 123 (2014) 151–157.
[4] H.C. Butterman, M.J. Castaldi, CO_2 as a carbon neutral fuel source via enhaned biomass gasification, Environ. Sci. Technol. 43 (23) (2009) 8.
[5] Y. Bai, Y. Wang, S. Zhu, L. Yan, F. Li, K. Xie, Synergistic effect between CO_2 and H_2O on reactivity during coal chars gasification, Fuel 126 (2014) 1–7.

[6] E.E. Kwon, Y.J. Jeon, H. Yi, New candidate for biofuel feedstock beyond terrestrial biomass for thermo-chemical process (pyrolysis/gasification) enhanced by carbon dioxide (CO_2), Bioresour. Technol. 123 (2012) 673–677.
[7] K. Açıkalın, F. Karaca, E. Bolat, Pyrolysis of pistachio shell: effects of pyrolysis conditions and analysis of products, Fuel 95 (2012) 169–177.
[8] L. Paetsch, C.W. Mueller, C. Rumpel, Š. Angst, A.C. Wiesheu, C. Girardin, N.P. Ivleva, R. Niessner, I. Kögel-Knabner, A multi-technique approach to assess the fate of biochar in soil and to quantify its effect on soil organic matter composition, Org. Geochem. 112 (2017) 177–186.
[9] Y. Yao, B. Gao, M. Inyang, A.R. Zimmerman, X. Cao, P. Pullammanappallil, L. Yang, Biochar derived from anaerobically digested sugar beet tailings: characterization and phosphate removal potential, Bioresour. Technol. 102 (10) (2011) 6273–6278.
[10] D. Angın, Effect of pyrolysis temperature and heating rate on biochar obtained from pyrolysis of safflower seed press cake, Bioresour. Technol. 128 (2013) 593–597.
[11] D.M. Keown, X. Li, J.I. Hayashi, C.Z. Li, Evolution of biomass char structure during oxidation in O_2 as revealed with FT-Raman spectroscopy, Fuel Process. Technol. 89 (12) (2008) 1429–1435.
[12] P. Fu, S. Hu, L. Sun, J. Xiang, T. Yang, A. Zhang, J. Zhang, Structural evolution of maize stalk/char particles during pyrolysis, Bioresour. Technol. 100 (20) (2009) 4877–4883.
[13] P. Fu, S. Hu, J. Xiang, L. Sun, S. Su, J. Wang, Evaluation of the porous structure development of chars from pyrolysis of rice straw: effects of pyrolysis temperature and heating rate, J. Anal. Appl. Pyrolysis 98 (2012) 177–183.
[14] F.A. López, T.A. Centeno, I. García-Díaz, F.J. Alguacil, Textural and fuel characteristics of the chars produced by the pyrolysis of waste wood, and the properties of activated carbons prepared from them, J. Anal. Appl. Pyrolysis 104 (2013) 551–558.
[15] A.C. Lua, F.Y. Lau, J. Guo, Influence of pyrolysis conditions on pore development of oil-palm-shell activated carbons, J. Anal. Appl. Pyrolysis 76 (1) (2006) 96–102.
[16] K. Zeng, D.P. Minh, D. Gauthier, E. Weiss-Hortala, A. Nzihou, G. Flamant, The effect of temperature and heating rate on char properties obtained from solar pyrolysis of beech wood, Bioresour. Technol. 182 (2015) 114–119.
[17] R.K. Sharma, J.B. Wooten, V.L. Baliga, M.R. Hajaligol, Characterization of chars from biomass-derived materials: pectin chars, Fuel 80 (12) (2001) 1825–1836.
[18] P.E.A. Debiagi, G. Gentile, M. Pelucchi, A. Frassoldati, A. Cuoci, T. Faravelli, E. Ranzi, Detailed kinetic mechanism of gas-phase reactions of volatiles released from biomass pyrolysis, Biomass Bioenergy 93 (Suppl C) (2016) 60–71.
[19] M. Van de Velden, J. Baeyens, A. Brems, B. Janssens, R. Dewil, Fundamentals, kinetics and endothermicity of the biomass pyrolysis reaction, Renew. Energy 35 (1) (2010) 232–242.
[20] K. Jamil, J.I. Hayashi, C.Z. Li, Pyrolysis of a Victorian brown coal and gasification of nascent char in CO_2 atmosphere in a wire-mesh reactor, Fuel 83 (7–8) (2004) 833–843.
[21] C. Guizani, F.J. Escudero Sanz, S. Salvador, Effects of CO_2 on biomass fast pyrolysis: reaction rate, gas yields and char reactive properties, Fuel 116 (2014) 310–320.
[22] H.S. Heo, H.J. Park, Y.-K. Park, C. Ryu, D.J. Suh, Y.-W. Suh, J.-H. Yim, S.-S. Kim, Bio-oil production from fast pyrolysis of waste furniture sawdust in a fluidized bed, Bioresour. Technol. 101 (1, Supplement) (2010) S91–S96.
[23] S.P. Gao, J.T. Zhao, Z.Q. Wang, J.F. Wang, Y.T. Fang, J.J. Huang, Effect of CO_2 on pyrolysis behaviors of lignite, J. Fuel Chem. Technol. 41 (3) (2013) 257–264.
[24] W. Huo, Z. Zhou, X. Chen, Z. Dai, G. Yu, Study on CO_2 gasification reactivity and physical characteristics of biomass, petroleum coke and coal chars, Bioresour. Technol. 159 (2014) 143–149.
[25] G. Wang, J. Zhang, X. Hou, J. Shao, W. Geng, Study on CO_2 gasification properties and kinetics of biomass chars and anthracite char, Bioresour. Technol. 177 (2015) 66–73.
[26] P. Basu, Biomass Gasification and Pyrolysis, Practical Design and Theory, Academic Press, 2010, pp. 38–41.
[27] Y. Bai, P. Wang, L. Yan, C. Liu, F. Li, K. Xie, Effects of CO_2 on gas evolution and char structure formation during lump coal pyrolysis at elevated pressures, J. Anal. Appl. Pyrolysis 104 (2013) 202–209.
[28] W.A.W.A.K. Ghani, A. Mohd, G. da Silva, R.T. Bachmann, Y.H. Taufiq-Yap, U. Rashid, A.a.H. Al-Muhtaseb, Biochar production from waste rubber-wood-sawdust and its potential use in C sequestration: chemical and physical characterization, Ind Crops Prod. 44 (2013) 18–24.
[29] H. Risnes, J. Fjellerup, U. Henriksen, A. Moilanen, P. Norby, K. Papadakis, D. Posselt, L.H. Sørensen, Calcium addition in straw gasification, Fuel 82 (6) (2003) 641–651.
[30] L. Lu, C. Kong, V. Sahajwalla, D. Harris, Char structural ordering during pyrolysis and combustion and its influence on char reactivity, Fuel 81 (9) (2002) 1215–1225.
[31] R. Rajarao, I. Mansuri, R. Dhunna, R. Khanna, V. Sahajwalla, Study of structural evolution of chars during rapid pyrolysis of waste CDs at different temperatures, Fuel 134 (2014) 17–25.
[32] W.T. Tsai, S.C. Liu, H.R. Chen, Y.M. Chang, Y.L. Tsai, Textural and chemical properties of swine-manure-derived biochar pertinent to its potential use as a soil amendment, Chemosphere 89 (2) (2012) 198–203.
[33] S. Kloss, F. Zehetner, A. Dellantonio, R. Hamid, F. Ottner, V. Liedtke, M. Schwanninger, M.H. Gerzabek, G. Soja, Characterization of slow pyrolysis biochars: effects of feedstocks and pyrolysis temperature on biochar properties, J. Environ. Qual. 41 (2012) 990–1000.
[34] X. Li, J.I. Hayashi, C.Z. Li, FT-Raman spectroscopic study of the evolution of char structure during the pyrolysis of a Victorian brown coal, Fuel 85 (12–13) (2006) 1700–1707.
[35] A. Sadezky, H. Muckenhuber, H. Grothe, R. Niessner, U. Pöschl, Raman microspectroscopy of soot and related carbonaceous materials: spectral analysis and structural information, Carbon 43 (8) (2005) 1731–1742.
[36] C.H. Chia, B. Gong, S.D. Joseph, C.E. Marjo, P. Munroe, A.M. Rich, Imaging of mineral-enriched biochar by FTIR, Raman and SEM–EDX, Vib. Spectrosc. 62 (2012) 248–257.